Diffusion and Kinetics of Solvent-Free Reaction between Molecular Crystals by Time-Resolved Powder UV−Vis Reflection Spectrum

Xin-Cun Tang,*,† Dian-Zeng Jia,*,‡ Chen-Kui Jiang,† Li-Hui Jiang,† and Zai-Ping Guo‡

College of Chemistry and Chemical Engineering, Center South University, Changsha 410083, China, and Institute of Applied Chemistry, Xinjiang University, Wulumuqi 830046, China

Received: March 2, 2008; Revised Manuscript Received: March 21, 2008

Traditionally, chemical reaction between solids has been considered to typically occur on a geological time scale without the benefit of high temperature, due to diffusion block in the solids. However, recent advancements have revealed that many solvent-free reactions between molecular crystals can quickly occur at room or near-room temperature. These reactions have raised a novel scientific question as to how the reactive species can overcome the diffusion-controlled kinetic limitations under such moderate conditions. From time-resolved powder UV−vis reflection spectra and optical micrographs with the reaction between dimethylglyoxime and $Ni(Ac)_2 \cdot 4H_2O$ and the reaction between hexamethylenetetramine and $CoCl_2 \cdot 6H_2O$ as models, we found that the solvent-free reaction really occurs at an intermediate state between the solid state and the liquid state. Formation of the liquid phase provides a convenient approach to diffusion of reactive species, whereas formation of a solid product layer hampered the transfer of reactive species. Both factors led to a broad reactive rate band in the long reaction region. The results have explained the diffusion mechanism of the fast reaction between the molecular crystals under moderate conditions.

1. Introduction

Chemical reactions between solids have been widely applied in the preparation of materials. Because of the diffusion limitations (because the diffusion coefficients in solids typically range from 10^{-12} to 10^{-16} cm^2/s) between the macroscopic solids, a long-held popular view is that the solid−solid reaction requires high thermal activation to overcome the barrier to transfer across the solid−solid interface.[1,2] Recently, however, a number of cases of the solvent-free reactions between molecular crystals occurring at moderate and even room temperature have been reported.[3–8] These cases have shown that many reactions occurring in the solution state can also be more simply carried out in the solvent-free state under very moderate conditions, even with a surprisingly high reaction rate and yield. Due to the advantage of solvent-free processing, the reactivity between molecular crystals has aroused wide interest because of its potential for green and low-cost synthesis,[9–12] especially for the preparation of the nanostructured materials.[13,14]

From the viewpoint of thermodynamics, if the change in the Gibbs free energy of the reaction system is less than zero, theoretically the reaction can occur, whether in the solution state or in the solvent-free state. In fact, not all reactions that can occur in the solution state can be favorably carried out in the solvent-free state. The diffusion-controlled kinetic limitations always play a more important role, because the reacting species have to diffuse across the solid product when the reaction product spatially separates the initial materials. According to the popular theory for solid reaction, defects or vacancies in the solids can provide an approach to transporting the reactive species at sufficiently high temperature.[15,16] Obviously, it cannot explain the high reaction rate and yield between molecular crystals in the solvent-free state at room or near-room temperature. Interestingly, many solvent-free reaction systems between molecular crystals that have been macroscopically observed involve the formation of a liquid phase during grinding of the solid reactants.[10,17,18] On the basis of the experimental observation of 19 organic examples, Scott et al.[19] even directly suggested that these solvent-free organic reactions occurred actually in a liquid melt. Anyway, these experimental facts at least suggested that there should be a special way of diffusion for the reactive species, which was dependent on the formation of the liquid phase and then leads to a high reaction rate and yield. However, to date, little is known how it affects the kinetics of the solvent-free reaction.

In this paper, we used the method of the time-resolved powder UV−vis reflection spectroscopy and optical metallography to respectively investigate the character of the reactive kinetics and diffusion mechanism between molecular crystals. Note that it is difficult for the X-ray diffraction (XRD) method to accurately track the variety of the reactive components by the intensity response of X-ray diffraction, because of the formation of a liquid phase during the reaction. Choosing the reaction between (DMG, white) and $Ni(Ac)_2 \cdot 4H_2O$ (blue) and the reaction between hexamethylenetetramine (HMT, white) and $CoCl_2 \cdot 6H_2O$ (red) as models for study is based on the obvious color contrast between the reaction components. Results suggest that the solvent-free reaction really occurs at an intermediate between the solid state and the liquid state. The formation of the micro liquid phase produces a convenient diffusion path to transfer the reactive species, which led to a broad reactive rate band in the long reaction region.

2. Theory on the Time-Resolved Powder UV−Vis Reflection Spectroscopy

As shown in Figure 1 light (I_0, the total intensity) incident upon solid matter will be partially reflected (I_R, the intensity of reflection), partially transmitted as a refracted ray (I_T, the

* To whom correspondence should be addressed. E-mail: tangxincun@163.com. Fax: +86-0731-8879616.
† Center South University.
‡ Xinjiang University.

10.1021/jp801835h CCC: $40.75
Published on Web 05/21/2008

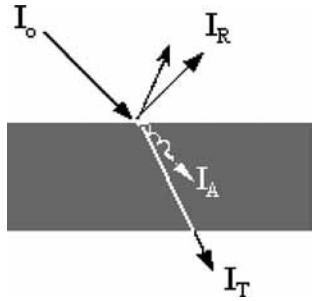

Figure 1. Schematic of the absorption, transmission, and reflection of light in a solid medium.

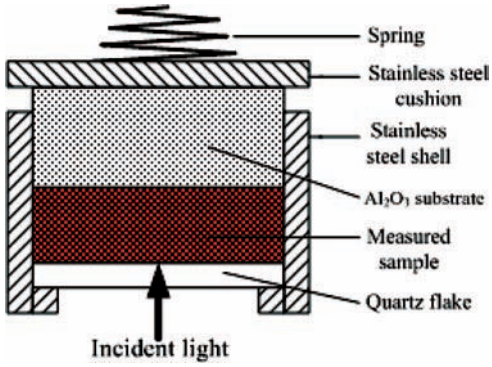

Figure 2. Assembly drawing of the groove.

intensity of transmission), and partially absorbed (I_A, the intensity of absorption) by the solid. If the solid matter is absolutely opaque, the value of I_T is zero. Thus,

$$I_0 = I_A + I_R \tag{1}$$

From eq 1, the powder UV−visible reflection spectrum can be transformed into the powder UV−visible absorbance spectrum. For incident light with constant wavelength (λ), if taking no account of the extra absorption resulting from the multiple internal reflection within the solid medium, according to the Lambert law, the absorbed-light density (D_A) is directly proportional to the concentration of the solid medium:

$$D_A = -\log \frac{I_A}{I_0} = \varepsilon_\lambda c \tag{2}$$

where ϵ_λ is a constant relative to the wavelength of the incident light and c is the concentration of the solid medium. Due to the effect of dispersion and internal reflection, D_A as a function of the thickness (l) of the solid medium is not fitted by the Beer law, and it can be expressed as[20]

$$\mathrm{d}D_A = m(D_{A,\infty} - D_A)\,\mathrm{d}l \tag{3}$$

$D_{A,\infty}$ is the absorbed-light density when the thickness (l) of the solid medium trends to ∞; m represents a constant relative to the surface features of the solid matter such as the smoothness and compactness. Combining the dependencies of D_A on concentration and thickness, as respectively given in eqs 2 and 3, D_A can be expressed as

$$\mathrm{d}D_A = \varepsilon_\lambda m(D_{A,\infty} - D_A)c\,\mathrm{d}l \tag{4}$$

If the solid medium is uniformly distributed in the range of the thickness l, eq 5 can be obtained by integrating eq 4:

$$\ln \frac{D_{A,\infty} - D_{A,0}}{D_{A,\infty} - D_A} = \varepsilon_\lambda mcl \tag{5}$$

Let

$$K_\lambda = \frac{\varepsilon_\lambda m}{A} \tag{6}$$

Here, A is the area where the incident light irradiates the solid medium, and its value is a constant, which is determined by the spectrophotometer. Therefore, K_λ is a constant relative to the wavelength of the incident light. Thus, eq 5 can be expressed as

$$\ln \frac{D_{A,\infty} - D_{A,0}}{D_{A,\infty} - D_A} = K_\lambda n \tag{7}$$

where n is the molar quantitiy of the solid medium in the volume of $A \times l$.

For the solvent-free reaction as follows:

$$b\mathrm{B} + c\mathrm{C} \rightarrow d\mathrm{D} + f\mathrm{F} \tag{8}$$

the reactive rate can be expressed as

$$v = -\frac{1}{b}\cdot\frac{\mathrm{d}n_B}{\mathrm{d}t} = -\frac{1}{c}\cdot\frac{\mathrm{d}n_C}{\mathrm{d}t} = \frac{1}{\mathrm{d}}\cdot\frac{\mathrm{d}n_D}{\mathrm{d}t} = \frac{1}{f}\cdot\frac{\mathrm{d}n_F}{\mathrm{d}t} \tag{9}$$

Combining eqs 7 and 9, the reactive rate v can be expressed as

$$v = \pm\frac{1}{K_\lambda}\mathrm{d}\left[\ln \frac{D_{A,\infty} - D_{A,0}}{D_{A,\infty} - D_A}\right]/\mathrm{d}t \tag{10}$$

Considering I_0 in eq 2 as a constant, eq 10 can be also expressed as

$$v = \pm\frac{1}{K_\lambda}\mathrm{d}\left[\ln \frac{\log(I_{A,0}/I_{A,\infty})}{\log(I_A/I_{A,\infty})}\right]/\mathrm{d}t \tag{11}$$

From eq 10 (or eqs 11 and 7), we can choose any one of the reactive components to obtain the kinetic curve of the reactive rate v versus the molar quantities n by time-resolved powder UV−visible reflection spectroscopy with "+" for product components and "−" for reactant components.

Through time-resolved powder UV−visible reflection spectroscopy, the kinetic data can be continuously determined with the smallest sampling interval of 0.2 s. Thus the details of the kinetic information can be perfectly recorded. Moreover, this method is also valid for the amorphous reaction system because the response of the absorbance intensity in the powder UV−visible reflection spectrum is not dependent on the crystallinity of the reactive components. These advantages are superior to those of the other methods, such as the XRD method, the intersection face moving method, etc.[21,22] In particular, the kinetic information in the initial stage of the reaction is difficult to obtain by the XRD method because of the small amounts of the reactive quantities.

3. Experimental Section

All time-resolved powder UV−visible absorption/reflection spectra were recorded on a Hitachi U-3010 spectrophotometer using Al_2O_3 as substrate. The measurement type is set as Time Scan, and the sampling interval time is set as 2 s. Before the experiments were carried out, all reactant grains were separately ground in an agate mortar for 20 min to produce fresh surface, and the particle size distribution of all reactants was less than 1 mm. The reactants with the theoretical molar ratio were quickly mixed by shaking the powder mixture in a little tube. The reaction occurred once the reactants were mixed, so the

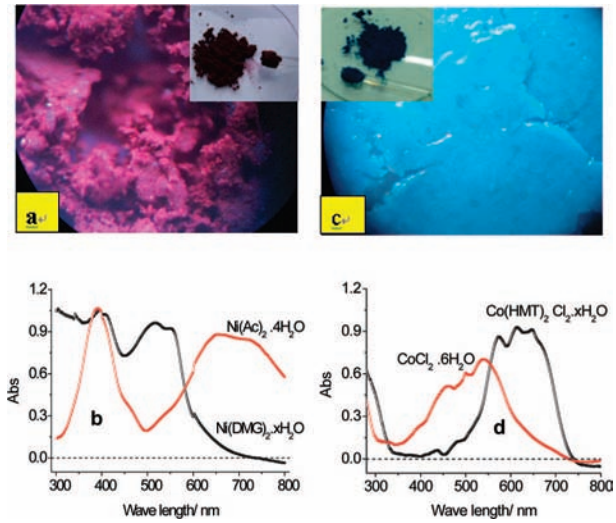

Figure 3. Optical Micrographs (×40) of mixture of DMG and $Ni(Ac)_2 \cdot 4H_2O$ (a) and mixture of HMT and $CoCl_2 \cdot 6H_2O$ (c). (b) and (d) are respectively the power UV−visible spectra of $Ni(Ac)_2 \cdot 4H_2O$ and $Ni(DMG)_2 \cdot xH_2O$, $CoCl_2 \cdot 6H_2O$ and $Co(HMT)_2Cl_2 \cdot xH_2O$. Dashed line in (b) and (d) is the background line deducted respectively the absorbance of DMG and HMT.

mixed samples had to be rapidly assembled into the special groove to carry out the measurement. For all spectral experiments, we controlled the operating time (from mixing to measuring) to be less than 20 s. An assembly drawing of the groove is shown in Figure 2. The low temperature operation of the measured samples was carried out in the BINDER MK53 Cold-/Heat Test Chamber (Germany).

Optical microscopy was performed with LEICA MEF3A/Quantimet 520/M optical metallography (OM). TG/DTA curves were recorded on a NETZSCH-449C thermal analyzer with a heating rate of 1 °C/min. The powder mixture of reactants was prepared for the TG/DTA determination as same as for the time-resolved powder UV−visible reflection spectra described above before the experiments were carried out.

4. Results and Discussion

Grinding the two reactants results in the formation of a liquid phase, as shown in Figure 3a,c, and respectively produces nickel(II) dimethylglyoximate (red) and cobalt(II) hexamethylenetetramate (blue). It can be seen from Figure 3b,d that there are two obviously contrasting absorption bands at about 520 nm in the absorption spectra of $Ni(Ac)_2 \cdot 4H_2O$ and $Ni(DMG)_2 \cdot xH_2O$, and at about 640 nm in the absorption spectra of $CoCl_2 \cdot 6H_2O$ and $Co(HMT)_2Cl_2 \cdot xH_2O$. Here, we respectively utilize variation of the absorbance at these absorption bands with time to study their solvent-free reaction kinetics.

Figure 4 shows the reactive kinetic curves of $K_\lambda v$ vs $K_\lambda n$, and the corresponding time-resolved powder UV−visible absorption spectra are given in the inset figure. It can be seen from the absorption spectra, as the reaction proceeds, that the response of the absorbance intensity increases with very high sensitivity. From the reactive kinetic curves in Figure 4, the maximum reactive rates are observed at the initial stage of the reaction. Both are almost lacking in reaction product dependency. At the initial stage, the transport of the reacting species is sufficiently fast at the interface of reactants or the very thin film of the product, which reflects a situation where the reactive kinetics exhibits the character of an interfacial solid−solid reaction obeying the linear reactive rate law.[23,24] Then the reactive rate sharply declines as the quantity of product increases. At this stage, the diffusion process becomes relevant, due to the increasing thickness of the reaction product layer. According to the general understanding of the solid−solid reaction, when the thickness of the reaction product layer increases to some extent, the diffusion completely determines the reaction rate, which reflects a situation where the reactive kinetics exhibits the character of theparabolic rate law.[25,26] To overcome the kinetic barrier, an elevated temperature is generally considered to enhance the diffusivity of the reacting species.[27] However, as the reaction proceeds further, a broad reactive rate band (marked by * in Figure 4) is unexpectedly observed in the long reaction region, which is different from the classical idea of the solid−solid reaction, as described above. Obviously, it is this broad reactive rate band that dominates the reactions between $CoCl_2 \cdot 6H_2O$ and HMT and between $Ni(Ac)_2 \cdot 4H_2O$ and DMG so that they can favorably proceed at room temperature. Here, the formation of the liquid phase due to the release of the crystal water in $Ni(Ac)_2 \cdot 4H_2O$ and $CoCl_2 \cdot 6H_2O$ has played an important role.

The optical micrographs in Figure 5 reveal the effect of the formation of a liquid phase on the characteristics of diffusion in the solvent-free reaction. It can be seen from the dashed circle in Figure 5a that there is a blue liquid region in the interface between the DMG and $Ni(Ac)_2 \cdot 4H_2O$, and the red $Ni(DMG)_2 \cdot xH_2O$ product (in the solid circle) covers the surface of the DMG. These features indicate clearly that the nickel(II) acetate diffuses to the surface of the DMG granules along the liquid region, and then the reaction occurs on the surface of the DMG. Because DMG remains in the solid state at the experimental temperature, the diffusion velocity of $Ni(Ac)_2 \cdot 4H_2O$ toward the surface of the DMG granules is much faster than that of DMG toward the surface of the $Ni(Ac)_2 \cdot 4H_2O$ granules. Thus, the site where the reaction occurs is the surface of the DMG, and consequently the $Ni(DMG)_2 \cdot xH_2O$ product is concentrated on the surface of the DMG. Parts b and c of Figure 5 respectively show optical micrographs of the initial and later stages of the reaction between.

HMT and $CoCl_2 \cdot 6H_2O$. Comparing (b) and (c) of Figure 5, we can clearly see that holes (as shown in the dashed circle in Figure 5c are left at the cluster sites of $CoCl_2 \cdot 6H_2O$ granules (as shown in the solid circle in Figure 5b) after the mixture of HMT and $CoCl_2 \cdot 6H_2O$ has reacted. These holes suggest that the diffusion between HMT and $CoCl_2 \cdot 6H_2O$ is not symmetrical during the reaction. Due to the release of the crystal water in $CoCl_2 \cdot 6H_2O$, the flow of $CoCl_2 \cdot 6H_2O$ toward HMT is much larger than that of HMT toward $CoCl_2 \cdot 6H_2O$. With $CoCl_2 \cdot 6H_2O$ continuously exhausted and the $Co(HMT)_2Cl_2 \cdot xH_2O$ products concentrated on the surface of the HMT, holes are left at the previous sites of $CoCl_2 \cdot 6H_2O$. These results show that the formation of the liquid phase produces a convenient diffusion path to transfer the reactive species. The endothermic peaks in Figure 5d,e suggest that the crystal water in $Ni(Ac)_2 \cdot 4H_2O$ and $CoCl_2 \cdot 6H_2O$ is released respectively at 39.4 and 25.8 °C in the powder mixture.[28] Figure 5f shows the reaction can still proceed even if the temperature is as low as −40 °C though the reactive rate become slower and the broad reactive rate band is tardily observed with the temperature decreasing. At the low temperature (such as −40 °C), the liquid phase is only formed by the reaction itself (for example, $x < 4$ for $Ni(DMG)_2 \cdot xH_2O$), which make the appearance of the broad reactive rate band need a longer time.

From Figure 4 the kinetic characteristics of the solvent-free reaction does not apparently follow the Arrhenins law. We can

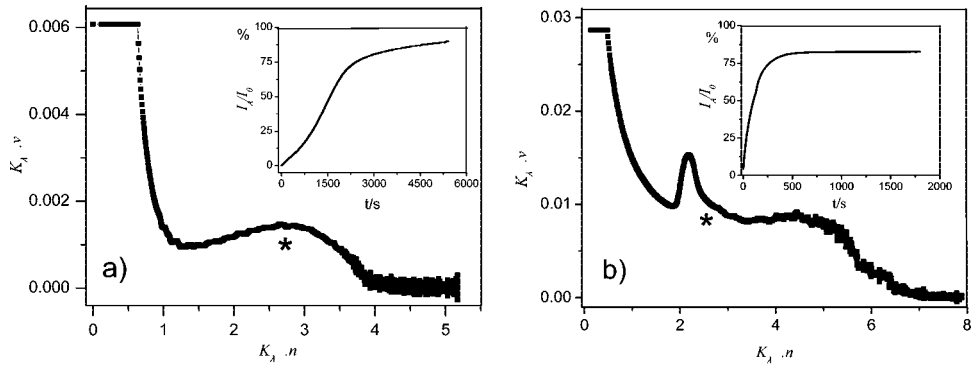

Figure 4. Curves of the reactive rate $K_\lambda v$ versus the molar quantity $K_\lambda n$ of the reaction (a) between $CoCl_2 \cdot 6H_2O$ and HMT and (b) between $Ni(Ac)_2 \cdot 4H_2O$ and DMG. Inset: corresponding time-resolved powder UV−visible absorption spectra measured respectively at the constant incident light wavelength of 640 nm (Figure 4a) and 520 nm (Figure 4b) and at 29 ± 1 °C.

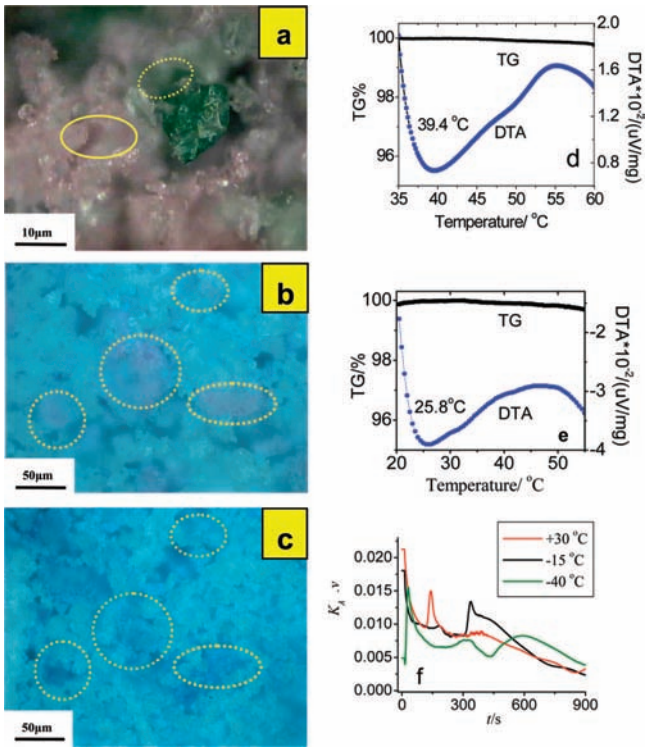

Figure 5. Optical micrographs taken at 26 ± 1 °C: (a) mixture of DMG (white) and $Ni(Ac)_2 \cdot 4H_2O$ (blue), with the red substance being the $Ni(DMG)_2 \cdot xH_2O$ products; (b) initial mixture of HMT (white) and $CoCl_2 \cdot 6H_2O$ (red, in the dashed circles), with the blue substance being the $Co(HMT)_2Cl_2 \cdot xH_2O$ products; (c) the holes left after the mixture of HMT and $CoCl_2 \cdot 6H_2O$ has reacted. None of the mixtures were ground before performing the above measurements. (d) Curves of the reactive rate $K_\lambda v$ versus time for the mixture of DMG and $Ni(Ac)_2 \cdot 4H_2O$ at different temperatures; (e) and (f) the TG/DTA curves of the mixture of DMG and $Ni(Ac)_2 \cdot 4H_2O$ and the mixture of HMT and $CoCl_2 \cdot 6H_2O$.

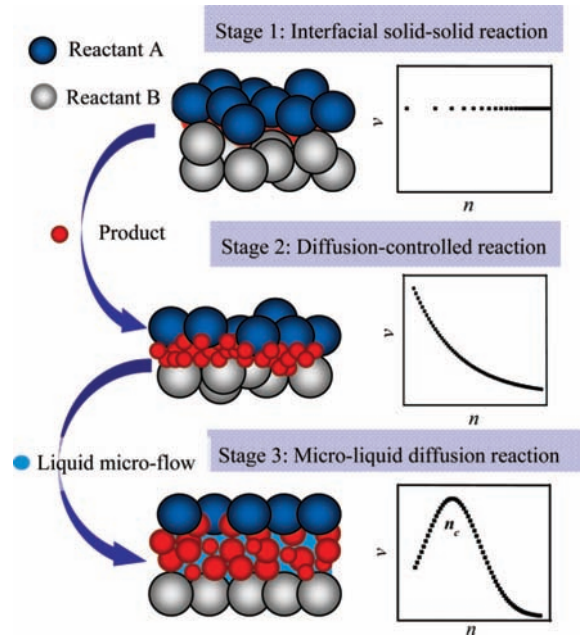

Figure 6. Schematic illustration of the typical solvent-free reaction between molecular crystals. The right curves exhibit the typical kinetic characteristics of each stage. n_c is the critical reactive quantity, where the reactive rate reaches a maximum value.

be divided into three distinct stages, as schematically shown in Figure 6. Initially, the reaction appears to be an interfacial solid−solid reaction with the constant reaction rate. Due to a little diffusional motions for the reactant molecules on the surface layer, the maximum reactive rates are observed at this stage. For the reaction as eq 8, assuming it is an elementary reaction, the reactive rate can be expressed as

$$v = k \cdot n_{Bi}^{\ b} \cdot n_{C,i}^{\ c} \qquad (12)$$

k is the constant of the reactive rate, and $n_{B,i}$ and $n_{C,i}$ respectively present the mole quantity of the reactant B and C at the reactive interface. At the initial stage of the interfacial solid−solid reaction, the reactive interface is almost on the surface of B and C particle. $n_{B,i}$ and $n_{C,i}$ are dependent on $n_{B,s}$ and $n_{C,s}$ (the mole quantity on the surface of B and C particle, which can be considered to be constant) and the effective contacted specific area (θ_{eff}) between the B and C particles, thus

$$v = k \cdot f(\theta_{eff}) \qquad (13)$$

Though the value of θ_{eff} is dependent on many factors such as the particle size, mixing uniformity and the ratio of reactants, etc., it is a fixed value at the given measurement condition. Therefore, the constant reaction rates are observed at the interfacial solid−solid reaction stage. This is followed by a solid diffusion-controlled reaction. In this stage, the reactive interface is far away from surface of B and C particle. Therefore, the reactant molecules have to diffuse across the solid product due to the increasing thickness of the reaction product layer. $n_{B,i}$ and $n_{C,i}$ are less than $n_{B,s}$ and $n_{C,s}$ according to the solid diffusion equation,[29] which leads to a decelerated reaction rate.

Fortunately, when the thickness of the reaction product layer increases to some extent, the reaction typically follows the

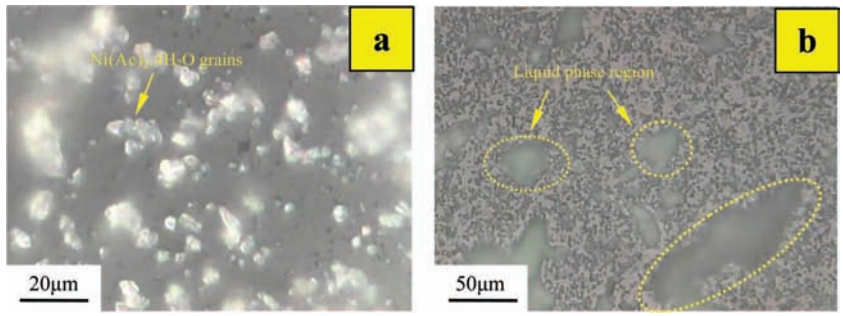

Figure 7. Polarized and transmitted light micrographs for the mixture of DMG and $Ni(Ac)_2 \cdot H_2O$ taken after (a) the mixture had reacted for 30 min at room temperature (26 ± 1 °C) without grinding and heating and (b) the mixture had reacted for 30 min at 50 °C.

microliquid diffusion mechanism, as shown in stage 3. In this stage, the liquid phase in the mixture can carry the reactive species to infiltrate through the reaction product layer; therefore it is beneficial to the diffusion of the reactants. Whereas, the reaction product layer can prevent the liquid phase from freely flowing. The reactive kinetics is dependent on both the quantity of the liquid phase and the thickness of the reaction product layer. As the reaction proceeds, both the quantity of the liquid phase and the thickness of the reaction product layer increase. There is a critical point at n_c, where the reactive rate reaches a maximum value. This is why the broad reactive rate bands are observed in Figure 4. However, the microliquid phase cannot flow as freely as a common solution, so strictly speaking, the reaction occurs really at an intermediate state between the solid state and the liquid state, because the thickness of the product layer is still an important unfavorable factor for the reactive kinetics. The polarized and transmitted light micrograph in Figure 7a shows that there still are many $Ni(Ac)_2 \cdot 4H_2O$ grains in the mixture, which suggests that the reaction between DMG and $Ni(Ac)_2 \cdot 4H_2O$ has not finished in 30 min at room temperature (26 ± 1 °C) without grinding and heating. Grinding or heating the reactant mixture are effective for increasing the reaction rate. Especially, heating the two solid reactants can accelerate the formation of liquid phase. As shown in Figure 7b, many liquid phase regions are observed in the mixture at 50 °C; and no $Ni(Ac)_2 \cdot 4H_2O$ grain is observed after 30 min reaction time. Considering the contribution of the microliquid diffusion reaction to the whole reaction, it is a reasonable viewpoint proposed by Scott et al.[19] that the formation of liquid phase is the precondition for a fast chemical reaction between solid molecular crystals. Generally, the molecular crystals have crystal water or low melting points, so that they can easily form the liquid phase under moderate conditions. We believe that most chemical reactions between molecular crystals, especially for organic synthesis, would be realized in an environmentally friendly manner by using the microliquid diffusion approach.

Acknowledgment. This work was supported by grants from the NNSF of China (No. 20406024 and No. 20676152).

References and Notes

(1) Fischer, D.; Jansen, M. *J. Am. Chem. Soc.* **2002**, *124*, 3488.
(2) Hedvall, J. A. *Solid State Chemistry*, (Elsevier: Amsterdam, 1966).
(3) Tanaka, K.; Toda, F. *Chem. Rev.* **2000**, *100*, 1025.
(4) Tanaka, K. *Solvent-free Organic Synthesis* (Wiley-VCH, 2003).
(5) Kaupp, G.; Schmeyers, J.; Boy, J. *Chemosphere.* **2001**, *43*, 55.
(6) Zhou, Y. M.; Xin, X.-Q. *Chinese J. Inorg. Chem.* **1999**, *15*, 273.
(7) Kaupp, G. *Curr. Opin. Solid State Mater. Sci.* **2002**, *6*, 131.
(8) Chen, T.; Liang, B.; Xin, X. *J. Solid State Chem.* **1997**, *132*, 291.
(9) Scheffer, J. R.; Scott, C. *Science.* **2001**, *291*, 1712.
(10) Epple, M.; Ebbinghause, S.; Reller, A.; Gloistein, U.; Cammenga, H. K. *Thermochim. Acta* **1995**, *269/270*, 433.
(11) Tang, X.-C.; Jiang, C.-K.; Pan, C.-Y.; Huang, B.-Y.; He, Y.-H. *J. Solid State Chem.* **2006**, *179*, 1100.
(12) Varma, R. S.; Dahiya, R. *J. Org. Chem.* **1998**, *63*, 8038.
(13) Wang, R. Y.; Jia, D. Z.; Zhang, L.; Liu, L.; Guo, Z. P.; Li, B. Q.; Wang, J. X. *Adv. Funct. Mater.* **2006**, *16*, 687.
(14) Ye, X. R.; Jia, D. Z.; Yu, J. Q.; Xin, X. Q.; Xue, Z. L. *Adv. Mater.* **1999**, *11*, 941.
(15) Maier, J. *Angew. Chem., Int. Ed. Engl.* **1993**, *32*, 528.
(16) Maier, J. *Angew. Chem., Int. Ed. Engl.* **1993**, *32*, 313.
(17) Tang, X.-C.; Huang, B.-Y.; He, Y.-H.; Jia, D.-Z. *Chin. J. Inorg. Chem.* **2004**, *20*, 795.
(18) Galway, A. K. *Thermochim. Acta* **1995**, *269/270*, 621.
(19) Rothenberg, G.; Downie, A. P.; Raston, C. L.; Scott, J. L. *J. Am. Chem. Soc.* **2001**, *123*, 8701.
(20) Lu, X.-G.; Huang, L.-G.; Cao, G.-H. Packing Chromatics; Printing Industry Press: Beijing, 2001. (Chinese).
(21) Belous, A. G.; Ovchar, O. V. *J. Mater. Res.* **2001**, *16*, 2350.
(22) Jing, S.; Xin, X.-Q. *Acta Chim. Sin.* **1995**, *53*, 26.
(23) Gösele, U.; Tu, K. N. *J. Appl. Phys.* **1982**, *53*, 3252.
(24) Johnson, W. C.; Martin, G. *J. Appl. Phys.* **1990**, *68*, 1252.
(25) Yudson, V. I.; Schulz, M.; Stepanow, S. *Phys. Rew. E* **1998**, *57*, 5053.
(26) Sung, Y. M.; Lee, Y. J.; Park, K.-S. *J. Am. Chem. Soc.* **2006**, *128*, 9002.
(27) Zhang, D. L.; Ying, D. Y. *Mater. Sci. Eng.* **2001**, *A301*, 90.
(28) Tang, X. C.; Huang, B. Y.; He, Y. H. *Chinese J. Inorg. Chem.* **2005**, *21*, 12.
(29) Evenson, W. E.; Decker, D. L. *Phys. Rew. B* **1978**, *17*, 583.

JP801835H